

Purdue University Purdue e-Pubs

International Refrigeration and Air Conditioning
Conference

School of Mechanical Engineering

2018

Comparison Of Approximation-assisted Component Modeling Methods For Steady State Vapor Compression System Simulation

Ransisi Huang

University Of Maryland, United States of America, cchuang5@umd.edu

Jiazhen Ling

University of Maryland, College Park, United States of America, jiazhen@umd.edu

Vikrant Chandramohan Aute

University of Maryland College Park, vikrant@umd.edu

Follow this and additional works at: <https://docs.lib.purdue.edu/iracc>

Huang, Ransisi; Ling, Jiazhen; and Aute, Vikrant Chandramohan, "Comparison Of Approximation-assisted Component Modeling Methods For Steady State Vapor Compression System Simulation" (2018). *International Refrigeration and Air Conditioning Conference*. Paper 1975.

<https://docs.lib.purdue.edu/iracc/1975>

This document has been made available through Purdue e-Pubs, a service of the Purdue University Libraries. Please contact epubs@purdue.edu for additional information.

Complete proceedings may be acquired in print and on CD-ROM directly from the Ray W. Herrick Laboratories at <https://engineering.purdue.edu/Herrick/Events/orderlit.html>

Comparison of Approximation-assisted Component Modeling Methods for Steady State Vapor Compression System Simulation

Ransisi HUANG¹, Jiazhen LING², Vikrant AUTE^{3*}

^{1,2,3} University of Maryland, Department of Mechanical Engineering,
College Park, Maryland, USA
Phone: ¹301-405-7314, ²301-405-8672, ³301-405-8726
Email: ¹cchuang5@umd.edu, ²jiazhen@umd.edu, ³vikrant@umd.edu

* Corresponding Author

ABSTRACT

When conducting a steady-state modeling of vapor compression cycle, an accurate, fast and robust heat exchanger model is critical for the robustness of the cycle simulation. In such simulations, the heat exchanger models are often the most time consuming components and moreover, if those models are black-box or third party provided, the simulations can be plagued by severe non-linearities. This paper investigates and compares two approximation-assisted (AA) heat exchanger (HX) modeling approaches, Kriging-based black box metamodel and kriging-assisted (AA) three zone model, with the distributed parameter approach being the baseline. The former approximates the heat exchanger behavior given a set of results from the baseline model. The latter approximates the lumped parameters of each phase, and calculates the outlet states based on energy conservation equations. To better understand the two methods, the approximated refrigerant side and airside results were verified using 10,000 operating points from an evaporator and a condenser. The verification shows that the mean deviation of pressure drop and enthalpy change is 1.65%, and 0.51% for the Kriging metamodel, and 1.56% and 1.41% for the three zone model. For both approximation-assisted models, the mean SHR deviation is 0.53%. For the condenser simulation, the approximation results show larger deviations when the HX outlet is two-phase and near saturation line. For the evaporator approximation, the three zone model causes larger deviation when the HX has non-uniform outlet enthalpy. The approximation-assisted modeling approaches were used in a steady-state, component-based system solver to simulate the performance of a four-component vapor compression system. With the Kriging metamodel, system coefficient of performance (COP) was under-predicted by 1.30%, 1.39% and 1.06% for ASHRAE A, B and C tests, respectively. With the three zone model, COP was over-predicted by 0.39%, 0.39% and 4.77% for the three tests respectively.

1. INTRODUCTION

Heat exchanger modeling approaches can be categorized into three classes: first principle based approach, black box approach and hybrid approach. First principle approach, e.g. distributed parameter model (Jiang *et al.*, 2006) requires detailed geometry information of the component and simulates the component performance based on thermodynamic laws and fundamental heat and mass transfer relations. It is accurate and offers the most insight into the component behavior, but meanwhile can be time-consuming. The black box approach approximates the component performance by formulating an input-output relation from a limited set of simulation or test data. The modeling technique of the black box approach includes the artificial neural networks (Zhao *et al.*, 2006, Li *et al.*, 2015) and statistical techniques such as polynomial regression (Sanaye *et al.*, 2004) and Gaussian process regression (Wen *et al.*, 2016). The black-box approach has low computational cost, but offers no underlying physics. By principle, it cannot be used for extrapolation. The hybrid approach takes advantage of the previous methods by lumping the physical and geometric information of the component into characteristic parameters, which are determined empirically on the basis of a training data set. Ding *et al.*, (2009) proposed a hybrid evaporator model in which the model parameters are approximated by linear or non-linear least-squares method.

The solution scheme for vapor compression system simulation can be categorized into the general equation scheme and the component-based scheme. In the general equation scheme, the mathematical equations for each component is evaluated and directly solved by the system solver. This scheme has good robustness but is obviously not flexible. The solver has to rewrite once the component details or system configuration change. In the component-based solution scheme, the system solver evaluates the system configuration and dynamically formulates a set of equations and

variables that are independent of the component models. The system-level equations are solved by numerical methods such as Newton-Raphson method and quasi-Newton method. Examples of the component-based scheme include the system simulation tool VapCyc[®] (Winkler *et al.*, 2008) and the comprehensive system solver (Beshr *et al.*, 2016). As opposed to the general equation scheme, this scheme provides flexibility in response to the change in system configuration and component details. Therefore, the component-based solution scheme is chosen in this paper for the comparison of different HX modeling approaches.

This paper aims to investigate and compare two different approximation-assisted air-to-refrigerant heat exchanger models for steady-state vapor compression system simulation, with the distributed parameter model being the baseline model. They are Kriging-based metamodel, a black-box approach, and approximation-assisted three zone model, a hybrid approach. The remainder of this paper is organized as following: Section 2 describes the approximation-assisted modeling methods. Section 3 presents the evaluation results of evaporator and condenser using the two models. Their deviations from the baseline results were reported and discussed. In section 4, the two HX modeling approaches were used in a steady-state, component-based system solver to simulate the performance of a four-component vapor compression system. The deviations of the system level results from the baseline results were reported for the two models, respectively.

2. APPROXIMATION-ASSISTED MODELING METHODS

2.1 Input Domain and Sampling

For both approximation methods, the refrigerant input state is specified by a three-dimensional vector \vec{x} whose components are pressure, enthalpy and mass flow rate. The input domain I , determined based on the heat exchanger operating conditions in a cycle, is given by

$$I = \begin{cases} I_e = \{ \vec{x} = (P, h, \dot{m}) \mid \text{evap inlet} \} \\ I_c = \{ \vec{x} = (P, h, \dot{m}) \mid \text{cond inlet} \} \end{cases} \quad (1)$$

The input domain can be estimated given the knowledge of airside operating conditions, degree of sub-cooling/superheat, and the compressor model (e.g. a 10-coefficient map). Figure 1 shows the flow chart to obtain the input domain I . Figure 2 shows an example of the projection of such a domain on the P-h diagram.

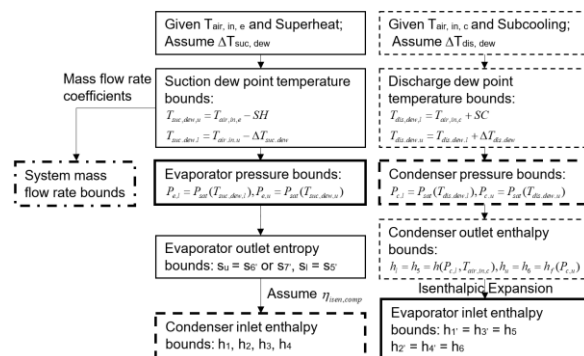


Figure 1 Flowchart of input domain estimation

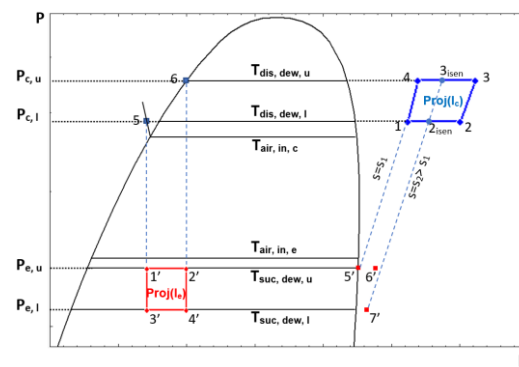


Figure 2 Projection of the input domain onto P-h diagram

The process of estimating I_e and I_c starts with determining the pressure bounds of evaporator and condenser, followed by determining condenser outlet enthalpy bounds and subsequently, evaporator inlet enthalpy bounds. The determination of condenser inlet enthalpy (discharge enthalpy) bounds requires the knowledge of evaporator outlet entropy (suction entropy) bounds. By following the isentropic lines on the P-h diagram (as shown in Figure 2), one can infer that discharge enthalpy would increase as the suction entropy increases. The lowest suction entropy should occur at 5' in Figure 2, or the saturation point along $P_{e,u}$. The highest suction entropy, depending on the refrigerant, may occur at 6' or 7', which can be determined by specifying the degree of superheat on $P_{e,u}$ and $P_{e,l}$, respectively. Next, the lower bounds of discharge enthalpy h_1 and h_4 are determined by assuming an isentropic compression from 5', the point at the highest suction entropy, to the pressure level of $P_{c,l}$ and $P_{c,u}$. Similar approach may be applied to locate $h_{2,isen}$, and $h_{3,isen}$, and by assuming the lowest isentropic efficiency, the actual upper bounds of discharge enthalpy, h_2 and h_3 can be determined.

Once the input domain is determined, 27 points are sampled using Latin Hypercube method. The sample library S is given by

$$S = \{\vec{x}^{(1)}, \vec{x}^{(2)}, \dots, \vec{x}^{(27)} \mid \vec{x}^{(i)} \in I, i = 1, 2, \dots, 27\} \quad (2)$$

The baseline heat exchanger model, based on the distributed parameter approach, will evaluate the 27 points and generate the result library R ,

$$R = \{\vec{y}^{(1)}, \vec{y}^{(2)}, \dots, \vec{y}^{(27)}\}. \quad (3)$$

2.2 Kriging-based Black-box Metamodel

For this modeling approach, the output in the result library, \vec{y} , is the overall pressure drop (ΔP), overall enthalpy change (Δh), and airside sensible heat ratio (SHR) evaluated by the baseline model at each sample point,

$$\vec{y}^{(i)} = (\Delta P, \Delta h, SHR) = f(\vec{x}^{(i)}), \vec{x}^{(i)} \in S, \vec{y}^{(i)} \in R \quad (4)$$

where $f(\vec{x}^{(i)})$ represents the input-output functional relation given by the baseline model. Though not required for successful cycle simulation, SHR is required for air-side prediction when dehumidification occurs. The 27 sets of inputs and outputs are fitted using Kriging into a metamodel \hat{f} , which provides a one-to-one mapping relation between the inputs within I and the heat exchanger outputs,

$$\hat{f}(\vec{x}) = \vec{y} = (\Delta P, \Delta h, SHR), \vec{x} \in I \quad (5)$$

The Kriging approach (Cressie, 1990; Jones *et al.*, 1998; Martin and Simpson, 2005) approximates computationally expensive functions by a stochastic process model given by,

$$\hat{f}(\vec{x}^{(i)}) = \mu + \varepsilon(\vec{x}^{(i)}) \quad (6)$$

where μ is the mean of the stochastic process, and $\varepsilon(\vec{x}^{(i)})$ is a normally distributed error term with mean zero. The errors at the sample points are assumed to be correlated. The most commonly used method in engineering design to describe the correlation between $\varepsilon(\vec{x}^{(i)})$ and $\varepsilon(\vec{x}^{(j)})$ is Gaussian function, which describes the correlation as negatively related to the distance between $\vec{x}^{(i)}$ and $\vec{x}^{(j)}$. In the Kriging approach, the Best Linear Unbiased Predictor (BLUP) is found by minimizing the mean square error (MSE) of the prediction, subjected to the unbiasedness constraint.

For simplicity, this modeling approach will be referred to as Kriging metamodel for the remaining sections.

2.3 Kriging-assisted Three Zone Model

Depending on the operating conditions of the heat exchanger, traditional three-zone model may divide the heat exchanger up to three zones. Heat transfer and hydrodynamics in each zone is characterized by a lumped overall heat transfer coefficient (U) and a lumped pressure drop (ΔP). In this hybrid approach, the output in the result library, \vec{y} , is U and ΔP of each phase, and SHR ,

$$\vec{y}^{(i)} = (\Delta P_{vap}, \Delta P_{tp}, \Delta P_{liq}, U_{vap}, U_{tp}, U_{liq}, SHR) = g(\vec{x}^{(i)}), \vec{x}^{(i)} \in S, \vec{y}^{(i)} \in R \quad (7)$$

where $g(\vec{x}^{(i)})$ represents the input-parameter functional relation from the baseline model. Then the data is fitted using Kriging into the parameter metamodel \hat{g} that maps the input into the key HX parameters that includes the lumped U and ΔP of each phase, and airside SHR ,

$$\hat{g}(\vec{x}) = \vec{y} = (\Delta P_{vap}, \Delta P_{tp}, \Delta P_{liq}, U_{vap}, U_{tp}, U_{liq}, SHR), \vec{x} \in I. \quad (8)$$

Figure 3 shows the flowchart of the Kriging-assisted three zone model. To unify the case of evaporator and condenser, phase indicator i is introduced. In the case of condenser, i would represent vapor phase ($i=1$), two phase ($i=2$) and liquid phase ($i=3$). For the evaporator, the definition of i is reversed, as shown in the table on the top-right corner in Figure 3. The initial value of the phase indicator would depend on the input \vec{x} . Usually, the calculation starts with $i = 2$ in the case of evaporator, and starts with $i=1$ in the case of condenser. Before the refrigerant side and airside energy calculation, the value of ΔP and U for each phase, and SHR are determined from the parameter metamodel. The refrigerant outlet states of each zone are calculated in sequence of the phase indicator i , until the accumulated phase length ($\sum_{j=1}^i L_j$) exceeds the total heat exchanger length L , or the calculation reaches the end of two-phase zone ($i = 2$). In either case, the length of the last phase will be the remaining HX length. The refrigerant outlet states of the

last zone, and the total HX capacity will be calculated accordingly. If the heat exchanger is an evaporator, the airside outlet enthalpy ($h_{o,air}$) and humidity ratio (w_o) will be calculated using the information of SHR and the total HX capacity, assuming no pressure drop. This modeling approach will be referred to as the three zone model for the remaining sections.

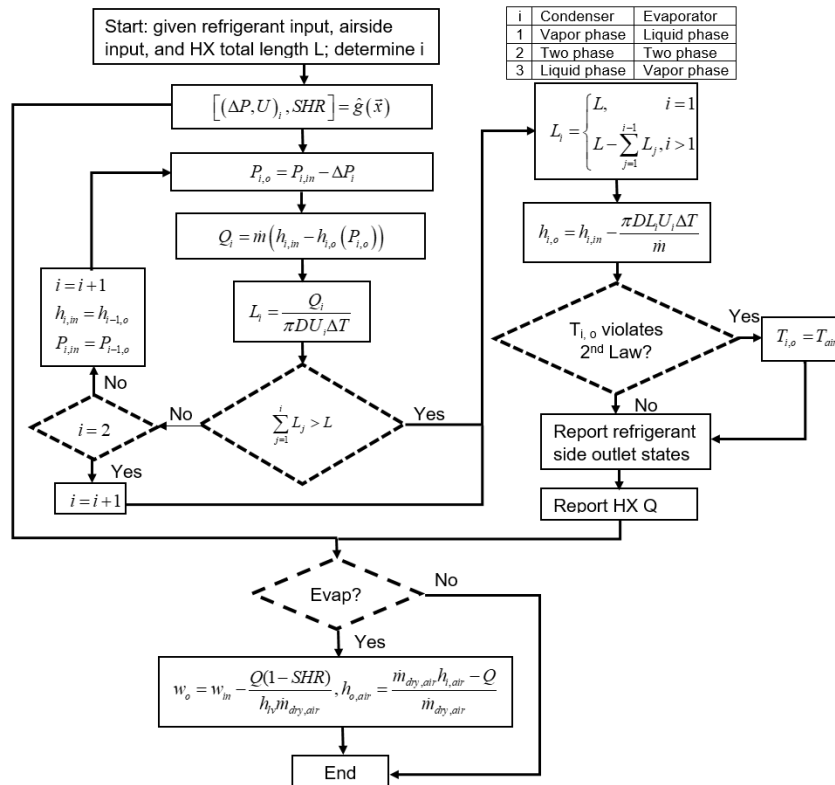


Figure 3 Flowchart of the Kriging-assisted three-zone heat exchanger model

3. VERIFICATION OF APPROXIMATION-ASSISTED HEAT EXCHANGER MODELS

3.1 Verification Method

Figure 4 (a) and (b) show the schematic of the heat exchangers used in the verification of the two approximation-assisted models. Alabdulkarem *et al.* (2015) described the geometry details and correlations for pressure drop and HTC calculations of the two heat exchangers. The refrigerant is R410A. Table 1 lists the inlet condition bounds in I_e and I_c . Table 2 tabulates the parameters required to determine the input domain for evaporator and condenser, I_e and I_c .

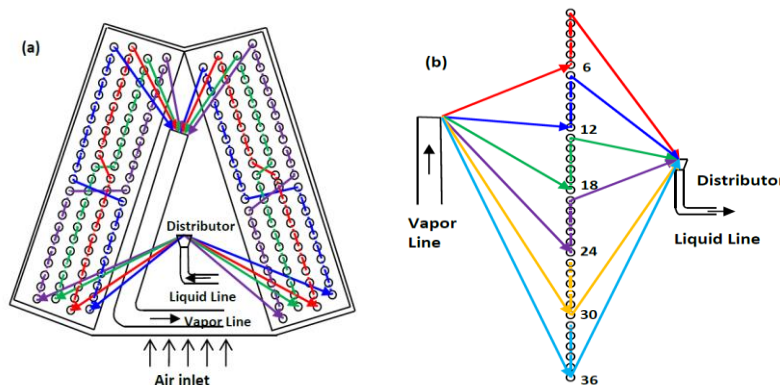


Figure 4: Schematic of HXs: a) evaporator, b) condenser

Table 1: Inlet Condition Bounds for Evaporator and Condenser

Inlet Condition	Evaporator		Inlet Condition	Condenser	
	min	max		min	max
P (kPa)	863.8	1116.0	P (kPa)	2537.7	3060.0
x (-)	0.18	0.36	T (K)	328	364
\dot{m} (kg/s)	0.044	0.062	\dot{m} (kg/s)	0.044	0.062

Table 2: Parameters for determination of I_e and I_c

Parameter	$\Delta T_{dis, dew}$ (K)	$\Delta T_{suc, dew}$ (K)	SC (K)	SH (K)	Compressor Model	$\eta_{isen, comp}$	$\Delta T_{air, c}$ (K)	$\Delta T_{air, e}$ (K)
Value	10	10	5	5	10-coefficient map	[0.7, 1]	308	299

Ten-thousand points were randomly selected within I_e and I_c , respectively. For each test point, the deviation between the baseline model results and the approximation assisted (AA) model results were calculated. The simulation results include the overall enthalpy change Δh , overall pressure drop ΔP , and sensible heat ratio (SHR). Enthalpy change deviation is given by

$$\delta_{\Delta h} = \left| \frac{\Delta h - \Delta h_{baseline}}{\Delta h_{baseline}} \right| \quad (9)$$

where Δh is the enthalpy change calculated by the AA model, and $\Delta h_{baseline}$ is the enthalpy change reported by the baseline model. Similarly, pressure drop deviation and SHR deviation are given by

$$\delta_{\Delta P} = \left| \frac{\Delta P - \Delta P_{baseline}}{\Delta P_{baseline}} \right| \quad (10)$$

$$\delta_{SHR} = \left| \frac{SHR - SHR_{baseline}}{SHR_{baseline}} \right| \quad (11)$$

3.2 Results and Discussion

Table 3 and 4 list the verification results of both AA models. In each table, deviations are categorized into five levels with 0~1% being the best and 20%+ being the worst. The verification results of pressure drop, enthalpy change and SHR are demonstrated by counting number of points fall into various categories. The mean deviation of pressure drop and enthalpy change is 1.65%, and 0.51% for the Kriging metamodel, and 1.56% and 1.41% for the three zone model. For both AA models, the mean SHR deviation is 0.53%. The approximation results by Kriging metamodel show 98.14% and 93.52% of evaporator domain and condenser domain is within 5% ΔP deviation. Moreover, 99.15% and 99.82% of evaporator domain and condenser domain is within 5% Δh deviation. As for the three zone model, 96.96% and 97.08% of evaporator domain and condenser domain is within 5% ΔP deviation. And 84.17% and 100% evaporator domain and condenser domain is within 5% Δh deviation. Therefore, for both AA models, enthalpy change approximation outperforms pressure drop approximation, and condenser approximation outperforms evaporator approximation.

Figure 5 (a) and (b) plot the Δh and ΔP deviation contour in the condenser input domain for Kriging metamodel, while Figure 5 (c) and (d) plot those contours for the three zone model. The ΔP deviation contours of both AA models share a similar pattern, presenting three main regions where ΔP deviation exceeds 5%. The first region is at the upper bound of \dot{m} and the lower bound of P_{in} . When the inlet condition falls in this region, the outlet condition is two-phase but near the saturation line. The second region is at the lower bound of \dot{m} and the upper bound of P_{in} . In this region, the low mass flow rate and high operating pressure lead to low pressure drop (1~2 kPa), so that the denominator in the deviation calculation becomes small. The third region is at small P_{in} , medium \dot{m} and the lower bound of h_{in} . Figure 5 (b) and (d) shows that for Kriging metamodel and three zone model, large Δh deviation ($\delta_{\Delta h} > 1\%$) occurs at the upper bound of \dot{m} and the lower bound of P_{in} . This region coincides with the first region where large ΔP deviation

occurs. Figure 5 (d) also shows that for the three zone model, large Δh deviation ($\delta_{\Delta h} > 1\%$) also occurs at the lower bound of h_{in} .

Similarly, Δh and ΔP deviation contours in evaporator input domain are plotted in Figure 6 (a)~(d). Figure 6 (a) and (c) show there are mainly two regions where ΔP deviation exceeds 5%. The first region is at the corner of \dot{m} upper bound, P_{in} upper bound and h_{in} lower bound. In this region, the outlet condition is two phase but there exists vapor phase in the coil. This indicates that in some circuits, the refrigerant is not fully vaporized. The second region is at the corner of \dot{m} upper bound, P_{in} upper bound and h_{in} upper bound. Figure 6 (b) shows for Kriging metamodel, the region where Δh deviation exceeds 5% is at the P_{in} upper bound, h_{in} upper bound and small \dot{m} . Figure 6 (d) shows that for the three-zone model, the maximum Δh deviation exceeds 20%, and large Δh deviation ($\delta_{\Delta h} > 5\%$) occurs at large \dot{m} , large P_{in} and small h_{in} . This region coincides with the first region with large ΔP deviation, and corresponds to those inlet conditions upon which some circuits are subjected to insufficient heat transfer from the air side and are thus not fully vaporized. Moreover Δh deviation shows clear trends of improvement as the inlet mass flow rate, inlet pressure and inlet enthalpy become smaller.

Table 3: Verification Result of Kriging Metamodel over I_e and I_c

Verification Indicator		$r = \Delta P_e$	$r = \Delta P_c$	$r = \Delta h_e$	$r = \Delta h_c$	$r = SHR$
$N(\delta_r \in X)$	$X = [0, 1\%)$	4273	4625	7000	9719	8422
	$X = [1\%, 5\%)$	5541	4727	2915	263	1578
	$X = [5\%, 10\%)$	186	641	85	18	0
	$X = [10\%, 20\%)$	0	7	0	0	0
	$X = [20\%, 1)$	0	0	0	0	0
Overall Deviation Statistics	$\bar{\delta}_r$	1.55%	1.74%	0.86%	0.15%	0.53%
		1.65%		0.51%		
	$\delta_{r,max}$	7.45%	11.78%	8.25%	6.83%	3.43%

Table 4: Verification Result of Three Zone Model over I_e and I_c

Verification Indicator		$r = \Delta P_e$	$r = \Delta P_c$	$r = \Delta h_e$	$r = \Delta h_c$	$r = SHR$
$N_{\delta_r \in X}$	$X = [0, 1\%)$	4310	4925	6851	9042	8422
	$X = [1\%, 5\%)$	5386	4783	1566	958	1578
	$X = [5\%, 10\%)$	304	278	677	0	0
	$X = [10\%, 20\%)$	0	14	882	0	0
	$X = [20\%, 1)$	0	0	24	0	0
Overall Deviation Statistics	$\bar{\delta}_r$	1.62%	1.50%	2.38%	0.44%	0.53%
		1.56%		1.41%		
	$\delta_{r,max}$	8.13%	13.50%	21.65%	3.99%	3.43%

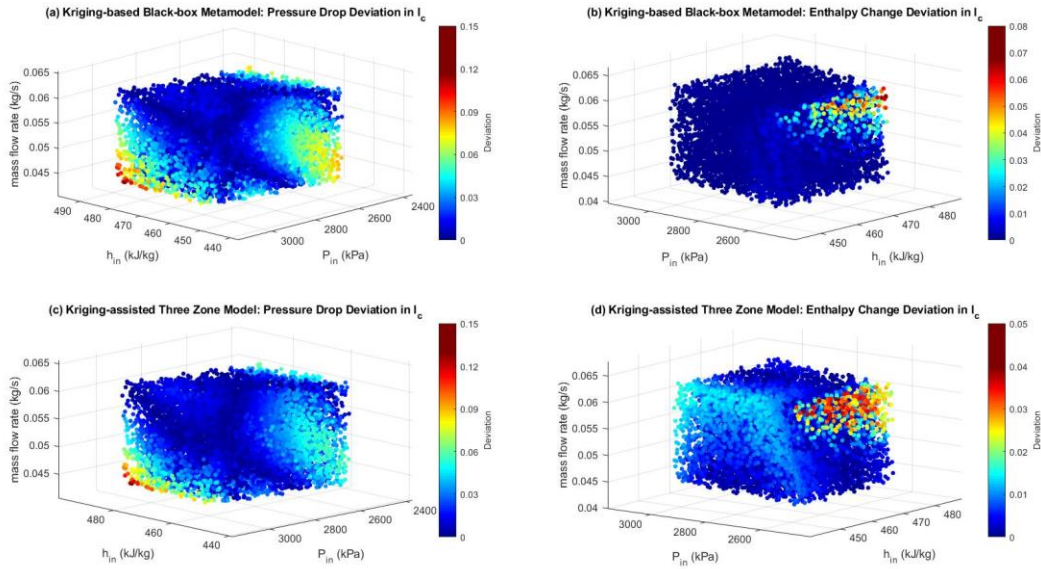


Figure 5: Contour of $\delta_{\Delta h}$ and $\delta_{\Delta P}$ in I_c

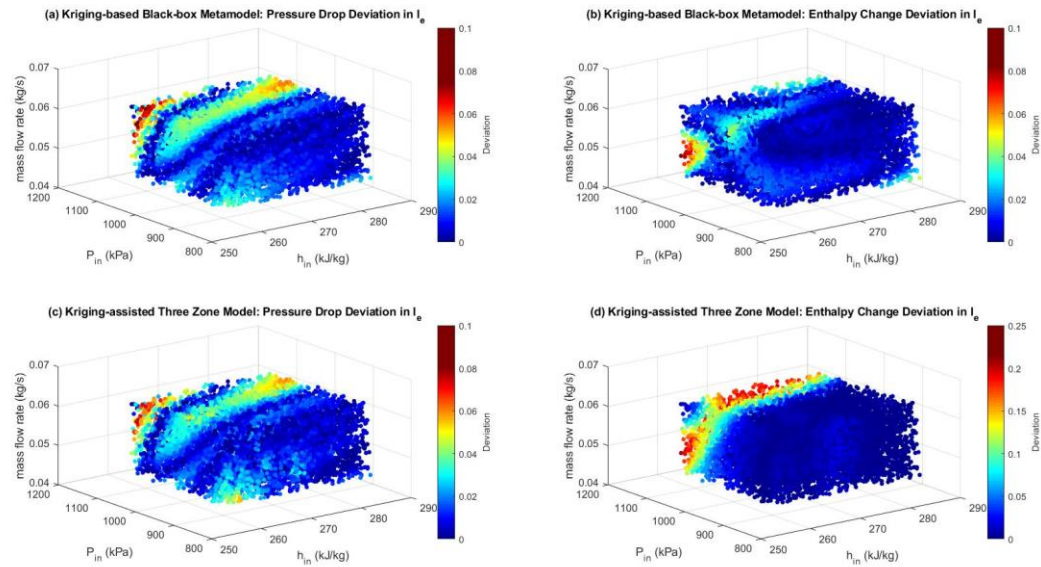


Figure 6: Contour of $\delta_{\Delta h}$ and $\delta_{\Delta P}$ in I_e

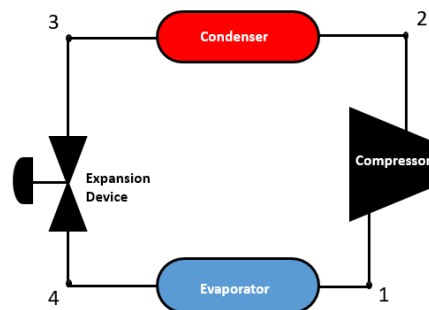
Table 5 shows the mean deviation and the maximum deviation of the airside results, which are the outlet temperature (dry-bulb) and the outlet relative humidity. It should be noted that the deviation here is defined as the absolute difference between the AA model result and the baseline result. The mean and maximum deviation is 0.64 K and 3.25 K for the outlet dry-bulb temperature, and 0.92% and 3.48% for the outlet relative humidity.

Table 5: Deviation statistics of airside results over I_e

Deviation Statistics ($\delta_r = r - r_{baseline} $)	$r = T_{o,db}$	$r = RH_o$
$\bar{\delta}_r$	0.64 K	0.92%
$\delta_{r,max}$	3.25 K	3.48%

4. COMPARISON OF VAPOR COMPRESSION SYSTEM SIMULATION RESULTS WITH APPROXIMATION-ASSISTED HEAT EXCHANGER MODELS

Figure 7 shows the schematic of a four-component vapor compression system, with state points labeled appropriately. It uses R410A as the refrigerant and its heat exchangers are listed in Figure 4. The degree of superheat and sub-cooling are both 5 K. Three test conditions were performed following ANSI/ASHRAE Standard 116 (2010). For test A and B (wet condition), outdoor dry-bulb temperatures are 308.15 K and 300.95 K, respectively, while the indoor dry-bulb and wet-bulb temperatures are 299.85 K and 292.55 K, respectively. For test C (dry condition), the outdoor dry-bulb temperature, indoor dry-bulb temperature and indoor wet-bulb temperatures are 300.95 K, 300.85 K and 284.15 K, respectively. The air flow rate for the condenser and the evaporator is 1.8 m³/s and 0.28 m³/s. The compressor is modeled using a 10-coefficient performance map.

**Figure 7:** Schematic of Vapor Compression System

This system was modeled with the baseline parameter-distributed HX model, Kriging metamodel, and the three zone model. A steady-state component-based system solver (Beshr *et al.*, 2016) is used to solve the cycle. The procedure with the two approximation-assisted models is as follows

1. Determine the input domain based on the method described in Figure 1.
2. Construct the sample library, run the sample points with the baseline HX model, and obtain the result library.
3. Use Kriging to fit the inputs and outputs from the sample and result library into the metamodel. For Kriging metamodel and the three-zone model, the target metamodel is Eq.(5) and Eq.(8), respectively.
4. Use the approximation-assisted model as the HX model in the steady state component-based system simulation solver.

Figure 8 shows the deviation of system results under ASHRAE test A, B and C conditions. With the Kriging metamodel, COP was under-predicted by 1.3%, 1.39% and 1.06% in test A, B and C, respectively. System capacity was under-predicted by 1.41%, 1.08% and 1.08% in test A, B and C, respectively. With the three zone model, COP was over-predicted by 0.39% in both test A and B, with the capacity being over-predicted by 0.16% and 1.08% in test A and B, respectively. The deviation of COP and capacity is 4.77% and 4.42% in test C. Figure 9 compares the P-h diagrams of the system predicted using the three HX models. The system P-h diagram predicted using the AA models is in good agreement with the baseline result in test A and B. In test C, the suction pressure is over-predicted by 3.87% using the three zone model, which leads to a -4.39% deviation in the difference between suction and discharge enthalpy, and a 4.24% deviation in mass flow rate. The two deviations cancel out and lead to -0.34% deviation in the power consumption. Moreover, the large capacity deviation in test C (4.42%) is not due to the deviation in state point prediction, but due to the over-prediction in mass flow rate.

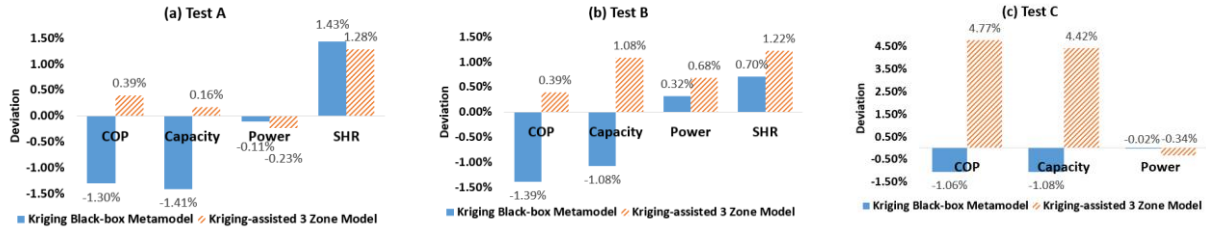


Figure 8: Deviation of System Results using Kriging Metamodel and Three Zone Model

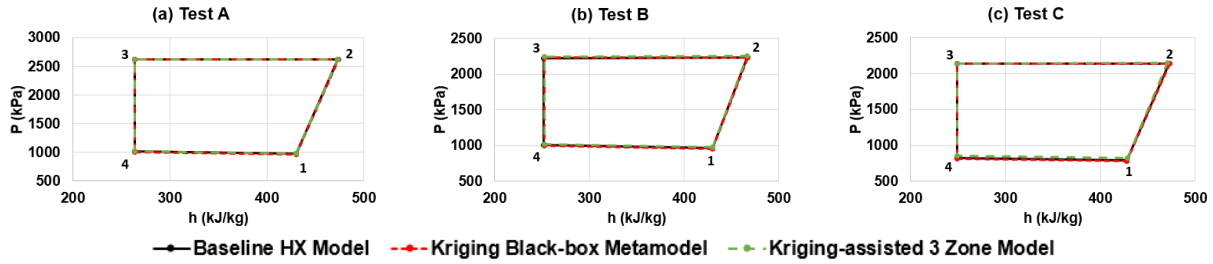


Figure 9: Comparison of System Result with different HX models on the P-h Diagram

5. CONCLUSIONS

In this paper, two approximation-assisted HX modeling approaches, Kriging-based metamodel (or Kriging metamodel) and kriging-assisted three zone model (or three zone model), were investigated and compared against the baseline distributed parameter model. The mean deviation, maximum deviation and the deviation contour of 10,000 testing points over condenser and evaporator domains were obtained. Moreover, a four-component vapor compression system was simulated using the two approximation-assisted models. The main conclusions are as following:

1. The mean deviation of pressure drop and enthalpy change is 1.65%, and 0.51% for the Kriging metamodel, and 1.56% and 1.41% for the three zone model. For both approximation-assisted models, the mean SHR deviation is 0.53%.

2. For Kriging metamodel and the three zone model, enthalpy change approximation outperforms pressure drop approximation, and condenser approximation outperforms evaporator approximation.

3. Kriging metamodel and the three zone model predict pressure drop and capacity with a larger deviation when the HX outlet is near saturation line. For the multi-circuit HX, the three zone model predicts enthalpy change with a larger deviation when the HX is operated at such inlet conditions that the outlet phases of the refrigerant in all circuits are not uniform.

4. With Kriging metamodel, COP was under-predicted by 1.30%, 1.39% and 1.06% under ASHRAE test A, B and C conditions. With the three zone model, COP was over-predicted by 0.39%, 0.39% and 4.77%. The system P-h diagrams predicted using Kriging metamodel in all three tests were in good agreement with the baseline result. Suction pressure was over-predicted by 3.87% using the three zone model in ASHRAE test C condition.

NOMENCLATURE

h	Enthalpy	I	Inlet condition domain
L	Heat exchanger length	\dot{m}	Mass flow rate
P	Pressure	Q	Capacity
R	Result library	S	Sample library
T	Temperature	U	Overall heat transfer coefficient
w	Humidity ratio	x	Quality
\vec{x}	Inlet condition	\vec{y}	Result library element
δ	Deviation	η	Efficiency
Abbreviation			
AA	Approximation-assisted	RH	Relative humidity

HX	Heat exchanger	SC	Sub-cooling
SH	Superheat	SHR	Sensible heat ratio
Subscript			
c	Condenser	db	Dry-bulb
dis, dew	discharge dew point	e	Evaporator
in	Inlet	isen	Isentropic
l	Lower bound	liq	Liquid phase
o	Outlet	suc, dew	Suction dew point
tp	Two phase	u	Upper bound
vap	Vapor phase		

REFERENCES

Jiang, H., Aute, V., & Radermacher, R. (2006). CoilDesigner: a general-purpose simulation and design tool for air-to-refrigerant heat exchangers. *International Journal of Refrigeration*, 29(4), 601-610.

Zhao, L. X., & Zhang, C. L. (2010). Fin-and-tube condenser performance evaluation using neural networks. *International Journal of Refrigeration*, 33(3), 625-634.

Li, Z. Y., Shao, L. L., & Zhang, C. L. (2015). Fin-and-tube condenser performance modeling with neural network and response surface methodology. *International Journal of Refrigeration*, 59, 124-134.

Sanaye, S., & Malekmohammadi, H. R. (2004). Thermal and economical optimization of air conditioning units with vapor compression refrigeration system. *Applied Thermal Engineering*, 24(13), 1807-1825.

Wen, J., Yang, H., Jian, G., Tong, X., Li, K., & Wang, S. (2016). Energy and cost optimization of shell and tube heat exchanger with helical baffles using Kriging metamodel based on MOGA. *International Journal of heat and Mass transfer*, 98, 29-39.

Ding, X., Cai, W., Jia, L., & Wen, C. (2009). Evaporator modeling—A hybrid approach. *Applied Energy*, 86(1), 81-88.

Winkler, J., Aute, V., & Radermacher, R. (2008). Comprehensive investigation of numerical methods in simulating a steady-state vapor compression system. *International Journal of Refrigeration*, 31(5), 930-942.

Beshr, M., Aute, V., & Radermacher, R. (2016). Steady State Modeling of Advanced Vapor Compression Systems. *International Refrigeration and Air Conditioning Conference*. Paper 1588.

Alabdulkarem, A., Eldeeb, R., Hwang, Y., Aute, V., & Radermacher, R. (2015). Testing, simulation and soft-optimization of R410A low-GWP alternatives in heat pump system. *International Journal of Refrigeration*, 60, 106-117.

Cressie, N. (1990). The origins of kriging. *Mathematical geology*, 22(3), 239-252.

Jones, D. R., Schonlau, M., & Welch, W. J. (1998). Efficient global optimization of expensive black-box functions. *Journal of Global optimization*, 13(4), 455-492.

Martin, J. D., & Simpson, T. W. (2005). Use of kriging models to approximate deterministic computer models. *AIAA journal*, 43(4), 853-863.

ACKNOWLEDGMENT

This work was supported by the Modeling and Optimization Consortium (MOC) at the University of Maryland.